TUM-HEP 1085/17
TTK-17-18

Co-annihilation without chemical equilibrium

Mathias Garny,[1] Jan Heisig,[2] Benedikt Lülf,[2] and Stefan Vogl[3]

[1] *Physik Department T31, Technische Universität München, James-Franck-Straße 1, D-85748 Garching, Germany*
[2] *Institute for Theoretical Particle Physics and Cosmology, RWTH Aachen University, Sommerfeldstraße 16, D-52056 Aachen, Germany*
[3] *Max-Planck-Institut für Kernphysik, Saupfercheckweg 1, D-69117 Heidelberg, Germany*

Chemical equilibrium is a commonly made assumption in the freeze-out calculation of co-annihilating dark matter. We explore the possible failure of this assumption and find a new conversion-driven freeze-out mechanism. Considering a representative simplified model inspired by supersymmetry with a neutralino- and sbottom-like particle we find regions in parameter space with very small couplings accommodating the measured relic density. In this region freeze-out takes place out of chemical equilibrium and dark matter self-annihilation is thoroughly inefficient. The relic density is governed primarily by the size of the conversion terms in the Boltzmann equations. Due to the small dark matter coupling the parameter region is immune to direct detection but predicts an interesting signature of disappearing tracks or displaced vertices at the LHC.

I. INTRODUCTION

The origin and the nature of the dark matter in the Universe is one of the most pressing questions in particle- and astrophysics. Despite impressive efforts to uncover the identity of dark matter and its interactions with the Standard Model (SM) of particle physics in direct detection experiments, a wide range of astrophysical observations and accelerator based experiments, dark matter remains elusive and, so far, our understanding is essentially limited to its gravitational interactions (see e.g. [1, 2]). It is therefore of utmost interest to investigate mechanisms for the generation of dark matter in the early Universe that go beyond the widely studied paradigm of thermal freeze-out, and that can point towards non-standard signatures.

In this spirit we subject the well-known co-annihilation scenario [3] to further scrutiny and investigate the importance of the commonly made assumption of chemical equilibrium (CE) between the dark matter and the co-annihilation partner. This requires solving the full set of coupled Boltzmann equations which has been done in the context of specific supersymmetric scenarios [4, 5]. Here we consider a simplified dark matter model and explore the break-down of CE in detail finding a new, conversion driven solution for dark matter freeze-out which points towards a small interaction strength of the dark matter particle with the SM bath. While the smallness of the coupling renders most of the conventional signatures of dark matter unobservable, new opportunities for collider searches arise. In particular we find that searches for long-lived particles at the LHC are very powerful tools for testing conversion-driven freeze-out.

The structure of the paper is as follows: We begin by introducing a simplified model for co-annihilating dark matter that we use as an instructive benchmark scenario in our analysis. In Sec. III we present the Boltzmann equations that govern the freeze-out of dark matter with a focus on the terms needed to describe departure from CE. Next, we investigate conversion-driven solutions to the Boltzmann equations and determine the regions of parameter space where freeze-out under out-of-chemical-equilibrium conditions can account for the dark matter in the Universe. In Sec. IV we confront the cosmologically preferred parameter space with LHC searches for the co-annihilation partner and, finally, we summarize our results in Sec. V. In the appendix we detail several technical aspects regarding the computation of the annihilation and conversion rates.

II. SIMPLIFIED MODEL FOR CO-ANNIHILATION

While the precise impact of the breakdown of CE between the dark matter and its co-annihilation partner will in general depend on the details of the considered model, the key aspects of the phenomenology can be expected to be universal. To investigate the freeze-out process quantitatively when relaxing the assumption of CE we therefore choose a simplified model for dark matter interacting with quarks as a representative case. We extend the matter content of the SM minimally by a Majorana fermion χ and a scalar quark-partner $\widetilde{q}$. The Majorana fermion χ, which we take to be a singlet under the SM gauge group, constitutes a good dark matter candidate while the scalar $\widetilde{q}$ mediates the interactions between the SM and the dark matter and also acts as its co-annihilation partner.

The interactions of the new particles among themselves and with the SM are given by [6]

$$\mathcal{L}_{int} = |D_\mu \widetilde{q}|^2 - \lambda_\chi \widetilde{q} q \frac{1-\gamma_5}{2}\chi + \text{h.c.}, \tag{1}$$

where q is a SM quark field, D_μ denotes the covariant derivative, which contains the interactions of $\widetilde{q}$ with the gauge bosons as determined by its quantum numbers, and λ_χ is a Yukawa coupling. In principle λ_χ is a free

parameter and we will vary it in our analysis. If we choose $q = b$, $\lambda_\chi = \frac{1}{3}\sqrt{2}\frac{e}{\cos\theta_W} \approx 0.17$ and $Y = -\frac{1}{3}$ our simplified model makes contact with the Minimal Supersymmetric Standard Model and the scalar quark partner can be identified with a right-handed sbottom and χ with a bino-like neutralino. From now on we will refer to the scalar mediator as sbottom and denote it by $\widetilde{b}$ even though it does not share all the properties of a super-partner of the b-quark. Note that choosing a top-partner instead yields similar results although quantitative differences arise due to the large top mass.

On top of the gauge and Yukawa interactions described above a Higgs-portal interaction given by

$$\mathcal{L}_h = \lambda_h h^\dagger h \widetilde{b}^\dagger \widetilde{b} \tag{2}$$

is also allowed. This interaction does not involve χ directly and has no impact on the conversion rates $\chi \leftrightarrow \widetilde{b}$, that are responsible for establishing CE. Nevertheless, it can modify the annihilation rate of $\widetilde{b}$. Since the additional contributions involving the scalar coupling compete with QCD processes, *i.e.* $\widetilde{b}\widetilde{b}^\dagger \to gg$, they are subleading unless λ_h is very large. Even in this case we do not expect qualitative differences, and therefore neglect this contribution in the following.

III. FREEZE-OUT WITHOUT CHEMICAL EQUILIBRIUM

For co-annihilation to be effective the co-annihilating particles – here χ and $\widetilde{b}$ – have to be in thermal contact through efficient conversion rates $\chi \leftrightarrow \widetilde{b}$. For couplings λ_χ of the order of the electroweak coupling strength, conversion rates are typically much larger than the Hubble rate H during freeze-out, guaranteeing CE, *i.e.* $n_\chi/n_\chi^{\rm eq} = n_{\widetilde{b}}/n_{\widetilde{b}}^{\rm eq}$. While CE holds the results are not sensitive to the size of the conversion rates (as long as they support CE) and the Boltzmann equations can be reduced to a single equation that does not contain conversion terms [7]. This approach is usually solved in standard tools [8–10].

For smaller couplings, however, CE can break down and the resulting freeze-out density becomes sensitive to the conversion rates. In this case the full coupled set of Boltzmann equations has to be solved [4, 5]. In our case it reads:

$$\begin{aligned}\frac{\mathrm{d}Y_\chi}{\mathrm{d}x} = \frac{1}{3H}\frac{\mathrm{d}s}{\mathrm{d}x}\Bigg[&\langle\sigma_{\chi\chi}v\rangle\left(Y_\chi^2 - Y_\chi^{\mathrm{eq}\,2}\right) + \left\langle\sigma_{\chi\widetilde{b}}v\right\rangle\left(Y_\chi Y_{\widetilde{b}} - Y_\chi^{\mathrm{eq}} Y_{\widetilde{b}}^{\mathrm{eq}}\right)\\ &+ \frac{\Gamma_{\chi\to\widetilde{b}}}{s}\left(Y_\chi - Y_{\widetilde{b}}\frac{Y_\chi^{\mathrm{eq}}}{Y_{\widetilde{b}}^{\mathrm{eq}}}\right) - \frac{\Gamma_{\widetilde{b}}}{s}\left(Y_{\widetilde{b}} - Y_\chi\frac{Y_{\widetilde{b}}^{\mathrm{eq}}}{Y_\chi^{\mathrm{eq}}}\right) + \left\langle\sigma_{\chi\chi\to\widetilde{b}\widetilde{b}^\dagger}v\right\rangle\left(Y_\chi^2 - Y_{\widetilde{b}}^2\frac{Y_\chi^{\mathrm{eq}\,2}}{Y_{\widetilde{b}}^{\mathrm{eq}\,2}}\right)\Bigg]\end{aligned} \tag{3}$$

$$\begin{aligned}\frac{\mathrm{d}Y_{\widetilde{b}}}{\mathrm{d}x} = \frac{1}{3H}\frac{\mathrm{d}s}{\mathrm{d}x}\Bigg[&\frac{1}{2}\left\langle\sigma_{\widetilde{b}\widetilde{b}^\dagger}v\right\rangle\left(Y_{\widetilde{b}}^2 - Y_{\widetilde{b}}^{\mathrm{eq}\,2}\right) + \left\langle\sigma_{\chi\widetilde{b}}v\right\rangle\left(Y_\chi Y_{\widetilde{b}} - Y_\chi^{\mathrm{eq}} Y_{\widetilde{b}}^{\mathrm{eq}}\right)\\ &- \frac{\Gamma_{\chi\to\widetilde{b}}}{s}\left(Y_\chi - Y_{\widetilde{b}}\frac{Y_\chi^{\mathrm{eq}}}{Y_{\widetilde{b}}^{\mathrm{eq}}}\right) + \frac{\Gamma_{\widetilde{b}}}{s}\left(Y_{\widetilde{b}} - Y_\chi\frac{Y_{\widetilde{b}}^{\mathrm{eq}}}{Y_\chi^{\mathrm{eq}}}\right) - \left\langle\sigma_{\chi\chi\to\widetilde{b}\widetilde{b}^\dagger}v\right\rangle\left(Y_\chi^2 - Y_{\widetilde{b}}^2\frac{Y_\chi^{\mathrm{eq}\,2}}{Y_{\widetilde{b}}^{\mathrm{eq}\,2}}\right)\Bigg],\end{aligned} \tag{4}$$

where $Y = n/s$ is the comoving number density, s the entropy density and $x = m_\chi/T$. We take the internal degrees of freedom $g_\chi = 2$ and $g_{\widetilde{b}} = 3$. $Y_{\widetilde{b}}$ represents the summed contribution of the sbottom and anti-sbottom. Since the cross sections are averaged over initial state degrees of freedom, this leads to the factor $1/2$ in Eq. (4). Equally, $\Gamma_{\chi\to\widetilde{b}}$ is understood to contain the conversion into both.

Apart from the familiar annihilation and co-annihilation terms, $\sigma_{\chi\chi}v$, $\sigma_{\chi\widetilde{b}}v$ and $\sigma_{\widetilde{b}\widetilde{b}^\dagger}v$, in the first lines of the Boltzmann equations three additional rates for the conversion processes enter. The first term in the second lines includes all the scattering processes which convert the dark matter in its co-annihilation partner. The scattering rate is given by

$$\Gamma_{\chi\to\widetilde{b}} = 2\sum_{k,l}\left\langle\sigma_{\chi k\to\widetilde{b}l}v\right\rangle n_k^{\mathrm{eq}}\,, \tag{5}$$

where k, l denote SM particles. The factor of two arises from annihilation into sbottom and anti-sbottom which give the same contribution. The next term captures the conversion induced by the decay and inverse decay of $\widetilde{b}$ and this rate is controlled by the thermally averaged decay width $\Gamma_{\widetilde{b}}$. Finally, the last term takes the scattering processes in the odd-sector into account. The rate is set by the thermally averaged annihilation cross section $\sigma_{\chi\chi\to\widetilde{b}\widetilde{b}^\dagger}v$. We include all diagrams that are allowed at tree-level. For more details regarding the included processes and the thermal averaging see App. A.

A first naive estimate that allows us to determine the ballpark of the parameters where conversion processes

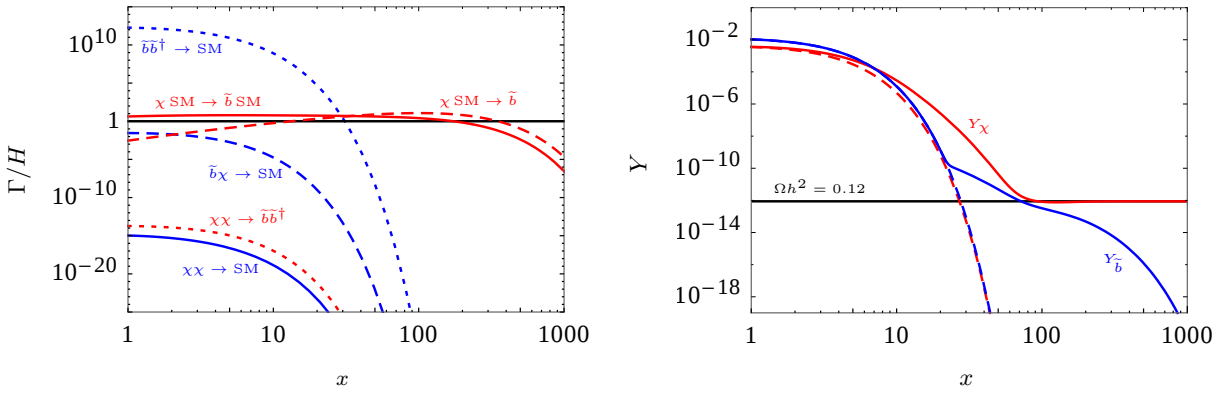

FIG. 1. Left panel: Rates of annihilation (blue curves) and conversion (red curves) terms in the Boltzmann equation relative to the Hubble rate as a function of $x = m_\chi/T$ for $m_\chi = 500\,\text{GeV}$, $m_{\tilde{b}} = 510\,\text{GeV}$, $\lambda_\chi \approx 2.6 \times 10^{-7}$. The thermal averages are shown for the direction $\chi \to \tilde{b}$, in particular the process $\chi\,\text{SM} \to \tilde{b}$ corresponds to the inverse decay rate $\Gamma_{\tilde{b}} Y_{\tilde{b}}^{\text{eq}}/Y_\chi^{\text{eq}}$. Right panel: Evolution of the resulting abundance (solid curves) of $\tilde{b}$ (blue) and χ (red). The dashed curves denote the equilibrium abundances.

become relevant for the evolution of the system can be obtained by demanding that

$$\Gamma_{\tilde{b}} \frac{Y_{\tilde{b}}^{\text{eq}}}{Y_\chi^{\text{eq}}} \sim H \,, \tag{6}$$

for temperatures relevant to the freeze-out dynamics ($m_\chi/T \sim 30$). Using as a representative benchmark $m_\chi = 500\,\text{GeV}$ and a value of the mediator mass that allows for co-annihilations (we choose $m_{\tilde{b}} = 510\,\text{GeV}$) this relation indicates $\lambda_\chi \sim \mathcal{O}(10^{-7})$. The order of magnitude is largely insensitive to the precise choice of masses, as long as co-annihilations can occur.

For such a small coupling a clear hierarchy emerges between the different rates, see left panel of Fig. 1. The annihilation $\chi\chi \to$ SM SM and $\chi\chi \to \tilde{b}\tilde{b}^\dagger$ that are proportional to λ_χ^4 and thermally suppressed by n_χ^{eq} are exceedingly small and can not compete with the Hubble expansion. Even though the co-annihilation rate $\chi\tilde{b} \to$ SM SM, which scales as $\sigma_{\chi\tilde{b}} v \propto \lambda_\chi^2 g^2$ (where g is a SM gauge coupling) is enhanced relative to this by many orders of magnitude it is also negligible compared to H. In contrast, the leading contribution to $\tilde{b}\tilde{b}^\dagger \to$ SM SM is set by the gauge interactions of $\tilde{b}$ and, therefore, the rate remains comfortably larger than H until $T \approx m_\chi/30$. The conversion rates are close to the Hubble rate and, for this choice of couplings, just about sufficient to make conversion processes relevant for the freeze-out.

Taking these rates and solving the Boltzmann equations we find the results presented in the right-hand side of Fig. 1. The χ abundance leaves its equilibrium value already at rather high temperatures, well before the freeze-out of a typical thermal relic or the $\tilde{b}$ freeze-out. The slow decline of the χ abundance after this point is due to the close-to inefficient conversion terms which remove over-abundant χs.

In Fig. 2 we show the dependence of the final freeze-out density on the coupling λ_χ (red solid line). For large enough coupling, the solution coincides with the result that would be obtained when assuming CE (blue dotted line). The relic density is in this case largely set by the strength of $\tilde{b}$ self-annihilation into gluons, with a large cross section given by the strong interaction. When lowering the value of λ_χ, conversions $\chi \leftrightarrow \tilde{b}$ become more and more inefficient. Since the χ abundance cannot be lowered as efficiently as in CE, we end up with a relic density that lies above the value expected for full CE. For the benchmark scenario shown in Fig. 2, the freeze-out density matches the value determined by Planck [11] for a coupling of $\lambda_\chi \approx 2.6 \times 10^{-7}$. In these and the following results we take into account Sommerfeld enhancement of the $\tilde{b}\tilde{b}^\dagger$ annihilation rates as described in App. B.

For the analysis above we assumed that both χ and $\tilde{b}$ have thermal abundances for $T \gg m_\chi$. While this assumption is certainly well justified for $\tilde{b}$, one may question the dependence on the initial condition for χ due to its small coupling to the thermal bath. We check the dependence on this assumption by varying the initial abundance at $T = m_\chi$ between $(0{-}100) \times Y_\chi^{\text{eq}}$. The evolution of the abundances for our benchmark point are shown in Fig. 3, for early times ($x < 20$). We find that all trajectories converge before $x \lesssim 5$, thereby effectively removing any dependence of the final density on the initial condition at $x = 1$ (for a discussion of kinetic equilibration, see App. A). The dependence of the final freeze-out density on the initial condition is also indicated in Fig. 2 by the area shaded in red, and is remarkably small. Therefore, conversion-driven freeze-out is largely insensitive to details of the thermal history prior to freeze-out and in particular to a potential production during the reheating process. Note that this feature distinguishes conversion-driven freeze-out from scenarios for which dark matter

has an even weaker coupling such that it was never in thermal contact (e.g. freeze-in production [12]). Thus, while requiring a rather weak coupling, the robustness of the conventional freeze-out paradigm is preserved in the scenario considered here.

As discussed before, conversions $\chi \leftrightarrow \widetilde{b}$ are driven by two types of processes, decay and scattering. It turns out that quantitatively both are important for determining the freeze-out density. To illustrate the importance of scattering processes, we show the freeze-out density that would be obtained when only taking decays into account by the gray dashed line in Fig. 2. Furthermore, the gray shaded area indicates the dependence on initial conditions that would result neglecting scatterings. We find that scattering processes, that are active at small x, are responsible for wiping out the dependence on the initial abundance in the full solution of the coupled Boltzmann equations.

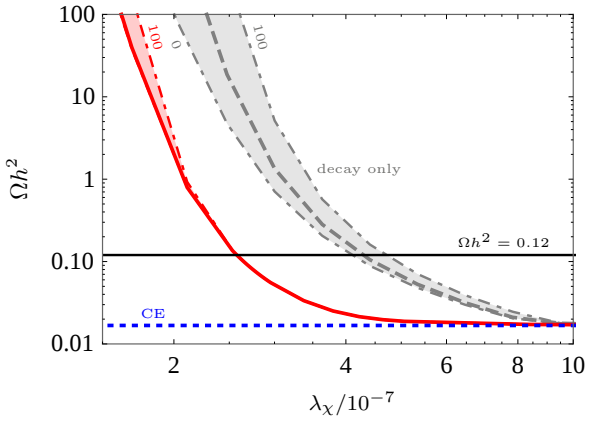

FIG. 2. Relic density as a function of the coupling λ_χ, for $m_\chi = 500\,\text{GeV}$, $m_{\widetilde{b}} = 510\,\text{GeV}$. The dotted blue line is the result that would be obtained when assuming CE. The red line shows the full solution including all conversion rates, the gray dashed line corresponds to the solution when only decays are considered. The shaded areas highlight the dependence on initial conditions, $Y_\chi(1) = (0-100) \times Y_\chi^{\text{eq}}(1)$. The central curves correspond to $Y_\chi(1) = Y_\chi^{\text{eq}}(1)$.

IV. VIABLE PARAMETER SPACE

We will now explore the parameter space consistent with a relic density that matches the dark matter density measured by Planck, $\Omega h^2 = 0.1198 \pm 0.0015$ [11]. In the considered scenario, for small couplings, $\widetilde{b}\widetilde{b}^\dagger$ annihilation is the only efficient annihilation channel. Hence the minimal relic density that can be obtained for a certain point in the m_χ-$m_{\widetilde{b}}$ plane is the one for a coupling λ_χ that just provides CE (but is still small enough so that $\chi\chi$- and $\chi\widetilde{b}$-annihilation is negligible). The curve for which this choice provides the right relic density defines the boundary of the valid parameter space and is

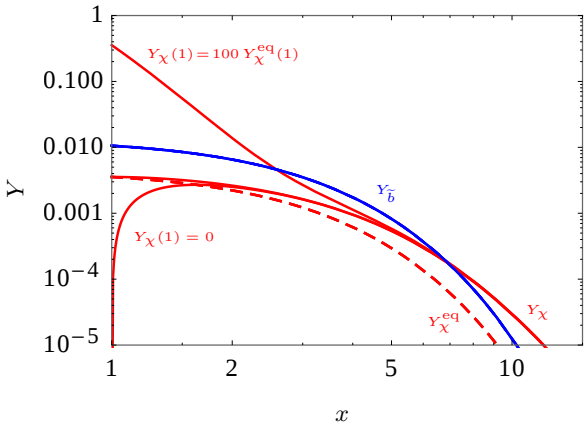

FIG. 3. Dependence on the initial conditions for Y_χ at $x = 1$. We show solutions for the choices $Y_\chi(1) = [0, 1, 100] \times Y_\chi^{\text{eq}}(1)$, and otherwise the same parameters as in Fig. 1.

shown as a black, solid curve in Fig. 4. Below this curve a choice of λ_χ sufficiently large to support CE would undershoot the relic density. In this region a solution with small λ_χ exists that renders the involved conversion rates just large enough to allow for the right portion of thermal contact between $\widetilde{b}$ and χ to provide the right relic density. The value of λ_χ ranges from 10^{-7} to 10^{-6} (from small to large m_χ). These values lie far beyond the sensitivity of direct or indirect detection experiments.

For the solutions providing the right relic density, during typical freeze-out (*i.e.* when $T \sim m_\chi/30$) the conversion rates have to be on the edge of being efficient, *cf.* Eq. (6). From this simple relation (and assuming that the decay width, $\Gamma_{\widetilde{b}}$, is similar in size as the other conversion rates) we can already infer that the decay length of $\widetilde{b}$ is of the order of 1–100 cm for a dark matter particle with a mass of a few hundred GeV. The decay length in our model is shown as the gray dotted lines in Fig. 4. It ranges from 25 cm to below 2.5 cm for increasing mass difference (the dependence on the absolute mass scale is more moderate). Below the gray dashed curve the 2-body decay is not allowed and the decay length is considerably larger.

In proton collisions at the LHC pairs of $\widetilde{b}$s could be copiously produced. They will hadronize to form R-hadrons [13] which will, for the relevant decay length, either decay inside or traverse the sensitive parts of the detector. Accordingly, the signatures of displaced vertices and (disappearing) highly ionizing tracks provide promising discovery channels at the LHC.

Due to the distinct signature of highly ionizing tracks the respective searches can be performed in a rather inclusive manner. They have been interpreted for lepton-like heavy stable charged particles (HSCPs) and R-hadrons [14–17]. Here we derive LHC constraints on the model by reinterpreting the results of [14] for detector-stable R-hadrons for finite decay lengths $c\tau$. To this end we compute the weighted fraction of R-hadrons that decay after traversing the relevant parts of the detector in a

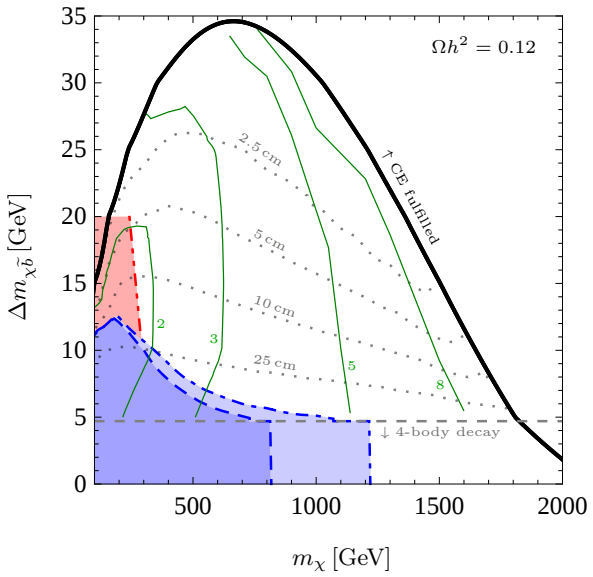

FIG. 4. Viable parameter space in the plane spanned by m_χ and $\Delta m_{\chi\tilde{b}} = m_{\tilde{b}} - m_\chi$. For each point we adjust λ_χ such that $\Omega h^2 = 0.12$. Above the thick black curve CE holds, while below this curve CE breaks down and solutions for the conversion-driven freeze-out exist. The corresponding coupling $\lambda_\chi/10^{-7}$ and decay length $c\tau$ of the sbottom is denoted by the thin green and gray dotted lines, respectively. The blue dashed and blue dot-dashed curves show our estimates for the limits from searches for R-hadrons at the 8 and 13 TeV LHC, respectively. The constraint from monojet searches at the 13 TeV LHC is shown as the red dot-dot-dashed curve. For mass splittings $\Delta m_{\chi\tilde{b}} < m_b$ the 2-body sbottom decay is kinematically forbidden and the sbottom becomes detector stable (below horizontal gray dashed line).

Monte Carlo simulation as follows. For a given R-hadron in an event i this fraction is

$$\mathcal{F}^i_{\text{pass}} = e^{-\ell/(c\tau\beta\gamma)}\,, \tag{7}$$

where $\ell = \ell(\eta)$ is the travel distance to pass the respective part of the detector which depends on the pseudo-rapidity η while γ is the Lorentz factor according to the velocity β. We use a simple cylindrical approximation for the CMS tracker[1] with a radius and length of 1.1 m and 5.6 m, respectively. For the weighting we compute[2]

$$\overline{\mathcal{F}}_{\text{pass}} = \frac{\sum_i \mathcal{F}^i_{\text{pass}} \mathcal{P}^i_{\text{on}} \mathcal{P}^i_{\text{off}}}{\sum_i \mathcal{P}^i_{\text{on}} \mathcal{P}^i_{\text{off}}}\,, \tag{8}$$

where $\mathcal{P}^i_{\text{on}}$ and $\mathcal{P}^i_{\text{off}}$ are the probabilities of the respective event to be triggered and pass the selection cuts, respectively, and the sum runs over all generated events. We use the tabulated probabilities $\mathcal{P}^i_{\text{on}}, \mathcal{P}^i_{\text{off}}$ for lepton-like HSCPs following the prescription in [18] (see also [19] for details of the implementation of isolation criteria and validation). We expect this to be a good approximation as the selection criteria for lepton-like HSCPs and R-hadrons are identical and differences in the overall detector efficiency cancel out in Eq. (8). We simulate events with MadGraph5_aMC@NLO [20], performing showering and hadronization with Pythia 6 [21].

We use the cross section predictions from NLL-fast [22] and rescale the signal by $\overline{\mathcal{F}}_{\text{pass}}$. The 95% CL exclusion limits are then obtained from a comparison to the respective cross section limits from searches for (top-squark) R-hadrons presented in [14]. The results are shown in Fig. 5. We show limits for two models regarding the hadronization and interaction of the R-hadron with the detector material, the generic model [23, 24] and Regge (charge-suppressed) model [25, 26] as the red solid and blue dashed line, respectively.

In addition to the results for the 8 TeV LHC we show results from an analogous reinterpretation of the preliminary results from 12.9 fb^{-1} of data from the 13 TeV LHC run [15]. Since the tabulated probabilities in [18] are only provided for 8 TeV we use these also for the analysis of the 13 TeV simulation assuming a similar detector efficiency for R-hadrons in both runs.

The fraction of R-hadrons passing the tracker is exponentially suppressed for small life-times significantly weakening the respective sensitivity. However, there are two competing factors that nevertheless result in meaningful limits for $c\tau$ smaller than the detector size. On the one hand, for small masses the production cross section rises quickly. On the other hand, for smaller masses a larger fraction of R-hadrons is significantly boosted enhancing the travel distance in the detector. How-

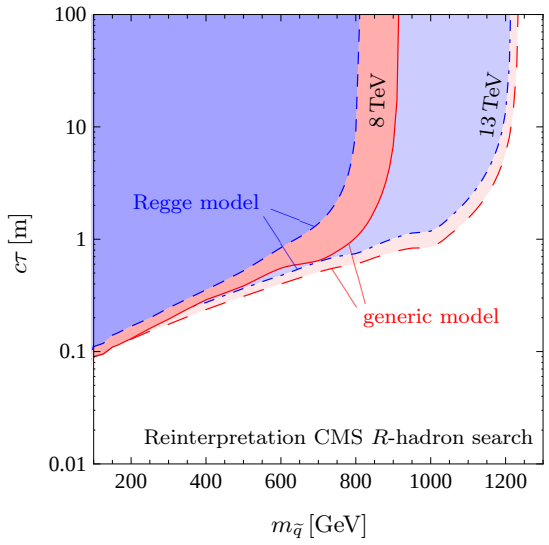

FIG. 5. Regions excluded at 95% CL by a reinterpretation of the searches for detector stable top-squark R-hadrons with CMS at the 8 TeV and 13 TeV LHC (tracker-only analysis).

[1] We considered the tracker-only and tracker+muon-system analysis of [14] finding the higher sensitivity for the former one.

[2] For simplicity we display the formula for one R-hadron candidates per event, for events with two candidates we follow the prescription in [18] (with the replacement $\mathcal{P}^i_{\text{off}} \to \mathcal{F}^i_{\text{pass}}\mathcal{P}^i_{\text{off}}$ in the respective sum in the numerator of Eq. (8)).

ever, this (latter) effect does not significantly enhance the sensitivity as the signal efficiency for largely boosted R-hadrons decreases rapidly (as tracks become indistinguishable from minimal ionizing tracks for $\beta \to 1$).

Note that the above CMS analysis has been interpreted for R-hadrons formed from top-squarks. As discussed in [26] the expected energy loss for an R-hadron containing sbottoms is smaller. This results in an efficiency around 30–40% smaller relative to the case of the stop and therefore in slightly weaker limits on the sbottom mass, see *e.g.* [16]. However, we use the above limit taking the result for the Regge model (that provides the weaker limits) as a realistic estimate of the LHC limits on sbottom-like R-hadrons considering the fact that the uncertainties in the hadronization model are of similar size as the difference between the sbottom and stop case.

The resulting limits are superimposed in Fig. 4. For mass splittings below m_b the 2-body decay is not allowed and the resulting R-hadrons can be considered detector-stable. Towards large mass splittings (smaller life-times) the limits fall off significantly providing no constraint above $\Delta m_{\tilde{\chi b}} \simeq 13\,\text{GeV}$. In this region a dedicated search for displaced vertices targeting decay lengths in the range 1–100 cm could significantly increase the sensitivity. Similar searches have, *e.g.*, been performed for a gluino R-hadron (decaying into energetic jets) [27] or a purely electrically charged HSCP [28, 29]. Displaced vertices in the context of simplified dark matter models have also been discussed in [30, 31].

Finally, let us note that a large number of experimental results for a sbottom-neutralino simplified model exist, *e.g.* [32–35], requiring a prompt sbottom decay which are not applicable to the scenario considered here. However, targeting small mass splittings between the sbottom and neutralino, monojet searches have been interpreted in the model that do not rely on the prompt decay of the sbottom [36, 37]. We superimpose the (stronger) limit from [37] that uses $3.2\,\text{fb}^{-1}$ of 13 TeV data.

V. CONCLUSION

In this work we have considered the possibility that the common assumption of chemical equilibrium during dark matter freeze-out does not hold. For definiteness, we have focused on a simplified model with particle content inspired by supersymmetry, comprising a neutral Majorana fermion as dark matter candidate and a colored scalar particle that mediates a coupling to bottom quarks. For small mass splitting between the mediator and the dark matter particle, the freeze-out is dominated by self-annihilation of the colored scalar. These can be efficient enough to deplete the dark matter density below the observed value, thus giving rise to a portion of parameter space in which thermal freeze-out cannot account for all of the dark matter abundance. In this work we have demonstrated that this conclusion hinges on the assumption of chemical equilibrium, and have shown that the freeze-out process can account for the dark matter density determined by Planck when relaxing this assumption. This occurs when the dark matter particle interacts very weakly with both the SM and the mediator, such that conversion processes have to be taken into account explicitly. We find that this opens up new regions in parameter space in which the final relic density is insensitive to the initial conditions and leads to characteristic signatures of long-lived particles at collider experiments. R-hadron searches performed at the 8 and 13 TeV LHC runs already constrain part of the parameter space providing conversion-driven freeze-out. A dedicated search for disappearing R-hadron tracks and displaced vertices targeting decay lengths in the range 1–100 cm is expected to probe an even larger portion of the allowed parameter space.

The mechanism discussed here is distinct from the freeze-in scenario [12], for which the dark matter particle was never in thermal equilibrium, and which would require a much smaller coupling strength than considered here. On the other hand, it shares some similarities with the superWIMP scenario (see *e.g.* [38]), but also differs in various respects. In particular, the relic density is set by the interplay of conversion and annihilation processes during freeze-out, unlike for superWIMPs, where dark matter is produced from the late decay of a heavier state that undergoes a standard thermal freeze-out. In addition, for the mechanism considered here, the life-time of the co-annihilation partner is short enough such that constraints from Big Bang nucleosynthesis are generally avoided, provided that the decay rate gives a sizeable contribution to conversion.

We expect that the mechanism described here can be realized generically in dark matter models featuring strong co-annihilations. Models comprising a strongly interacting co-annihilation partner and a dark matter particle with much weaker interactions lead to R-hadron signatures similar to the one discussed here. If the co-annihilation partner is instead color neutral, but only electrically charged, one may expect signatures related to lepton-like highly ionizing tracks. Finally, it is possible that the efficient self-annihilation of the co-annihilation partner is itself driven by a new interaction beyond the SM [39]. In this case the mechanism described here can be relevant even if the co-annihilating state is a SM singlet with macroscopic decay length, potentially leading to displaced vertex signatures.

ACKNOWLEDGEMENTS

We thank Michael Krämer, Björn Sarrazin, Pasquale Serpico and Wolfgang Waltenberger for helpful discussions. We acknowledge support by the German Research Foundation DFG through the research unit "New physics at the LHC".

Appendix A: Annihilation and conversion rates

We use FeynRules [40] and CalcHEP [41] to generate the squared matrix elements $|\overline{M}|^2$. The considered processes for annihilation and conversion are shown in Tabs. I and II. The most important annihilations, especially for very small λ_χ are the $\widetilde{b}$ annihilations into gluons. Since the interaction rates are suppressed exponentially by the masses of external particles, it is clear that the conversion processes containing external gluons dominate over the rates containing weak scale particles.

At low temperatures $x \gtrsim \mathcal{O}(10)$ the (inverse-)decay $\widetilde{b} \leftrightarrow b\chi$ contributes substantially to the conversion rate. Neglecting quantum statistical factors and assuming Boltzmann distributions, the thermally averaged decay rate is given by

$$\Gamma_{\widetilde{b}} \equiv \Gamma \left\langle \frac{1}{\gamma} \right\rangle = \Gamma \frac{K_1\left(m_{\widetilde{b}}/T\right)}{K_2\left(m_{\widetilde{b}}/T\right)} \,, \tag{A1}$$

where γ is the Lorentz factor and K_i are modified Bessel function of the second kind. For annihilation and scattering the thermal averages read [7]

$$\langle \sigma_{ij} v \rangle \, n_i^{\rm eq} n_j^{\rm eq} = T \frac{g_i g_j}{256\pi^5} \int \frac{p_{ij} p_{ab}}{\sqrt{s}} |\overline{M}|^2 K_1\left(\frac{\sqrt{s}}{T}\right) \mathrm{d}s \, \mathrm{d}\cos\theta \,. \tag{A2}$$

Here g_i are the internal degrees of freedom of species i, p_{ij} and p_{ab} denote the absolute value of the three momentum of the initial and final state particles in the center-of-mass frame, respectively. Due to the inclusion of scattering processes, two issues arise in the thermal averages. Since we do not consider loop corrections to the two-body decay or $1 \to 3$ processes $\widetilde{b} \to \chi b g$, we cannot use them to cancel soft contributions from $g\widetilde{b} \leftrightarrow b\chi$ scatterings (of course, also the γ scattering has this problem, noted by * in Tab. II). Instead, we regularize these processes by imposing a cut on the minimal process energy of $s_{\rm min} = (m_{\widetilde{b}} + m_{\rm cut})^2$, with fiducial value $m_{\rm cut} = 0.5\,\mathrm{GeV}$. We checked that our numerical results are stable when varying $m_{\rm cut}$ over a wide range, see Fig. 6, indicating that the bulk of the scattering processes occurs at energies above the b mass. On top of this, we find that in processes of the type $\widetilde{b}\bar{b} \leftrightarrow \chi H$ the b-quark in the t-channel is allowed to go on-shell for some center-of-mass energies (the affected processes are marked with ** in Tab. II). This corresponds to a double counting of the on-shell two-body decay. We choose to suppress the on-shell part by introducing a large Breit-Wigner width for the b-quark, taking $\Gamma_b = m_b$ in our numerical calculations. Since this issue occurs only in processes involving weak scale particles (H, W, Z) and the scattering rate is dominated by gluons the precise value for the width does not have an appreciable impact on the results. We solve the system of coupled equations from $x = 1$ up to $x = 1000$. Due to efficient annihilations, the $\widetilde{b}$ abundance is very close to equilibrium at early times. For numerical convenience, it is sufficient to track its deviation from equilibrium starting from $x \sim 15$.

initial state		final state		scaling
χ	χ	b	$\bar{b}$	λ_χ^4
χ	$\widetilde{b}$	b	g, γ, Z, H	λ_χ^2
		W^-	t, u, c	
$\widetilde{b}$	$\widetilde{b}^\dagger$	V	V	λ_χ^0
		q	$\bar{q}$	
		l	$\bar{l}$	
$\widetilde{b}$	$\widetilde{b}$	b	b	λ_χ^4

TABLE I. List of all included co-annihilation processes. We use the abbreviations q = all quarks, l = all leptons and $V = g, \gamma, Z, W$. The $\widetilde{b}$ annihilation into $b\bar{b}$ also has contributions scaling with λ_χ^2 and λ_χ^4.

initial state		final state		symbol	scaling
χ	b	$\widetilde{b}$	g^*, γ^*, Z, H	$\Gamma_{\chi\to\widetilde{b}}$	λ_χ^2
	$g, \gamma, Z^{**}, H^{**}$		$\bar{b}$		
	W^-		$\bar{t}, \bar{u}^{**}, \bar{c}^{**}$		
	t^{**}, u, c		W^+		
$\widetilde{b}$		χ	b	$\Gamma_{\widetilde{b}}$	λ_χ^2
χ	χ	$\widetilde{b}$	$\widetilde{b}^\dagger$	$\langle\sigma_{\chi\chi\to\widetilde{b}\widetilde{b}^\dagger} v\rangle$	λ_χ^4

TABLE II. List of all considered conversion processes. Processes marked with * have soft divergences, processes with ** can have t-channel divergences.

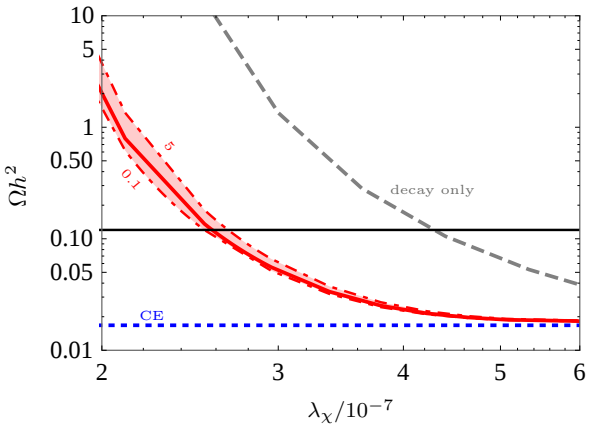

FIG. 6. Dependence of the final dark matter density on the regularization parameter $m_{\rm cut} \in [0.1, 0.5, 5]\,\mathrm{GeV}$, for $m_\chi = 500\,\mathrm{GeV}$, $m_{\widetilde{b}} = 510\,\mathrm{GeV}$.

Let us briefly comment on possible refinements. Apart from quantum statistics, also thermal effects could play a

role at small x. In particular, the thermal mass for the b-quark can lead to a thermal blocking of the decay at high temperatures and for very small mass splitting. Since a consistent inclusion of this effect would require to take also further thermal processes into account, and since (hard) scatterings dominate for small x, we do not expect these corrections to significantly affect our conclusion. Additionally, bound state effects could play a role for the $\widetilde{b}$ annihilation [42, 43].

Since χ is very weakly coupled to the thermal bath of SM particles, one may wonder whether it is justified to describe its distribution function by a thermal distribution. While a detailed answer goes beyond the scope of this work, and is partly model dependent, we present several arguments that justify this assumption: (i) for small x scattering processes involving χ are in equilibrium. Such processes also establish kinetic equilibrium. (ii) if the χ particle is produced from the thermal bath, its distribution is (close to) thermal even if kinetic equilibrium does not hold. (iii) there may be further, heavier particle species, like e.g. a further colored scalar $\widetilde{q}$ that couples χ to the other SM quarks $q \neq b$ with strength $\lambda_{\widetilde{q}}$, that establish thermal equilibrium at $T \gg m_\chi$. At the temperatures relevant to freeze-out such additional states would mediate a dimension-6 interaction $\mathcal{L} \propto \frac{1}{\Lambda^2}\bar{\chi}\chi\bar{q}q$, where $\Lambda \sim m_{\widetilde{q}}/\lambda_{\widetilde{q}}$. We checked that for values of Λ for which this interaction can maintain kinetic equilibrium up to at least $x \sim 30$, it does not affect the freeze-out density.

Appendix B: Sommerfeld enhancement

In the presence of light degrees of freedom non-perturbative corrections to the annihilation rates are known to become relevant in the non-relativistic limit [44, 45]. Between pairs of color charged particles the exchange of gluons generates a potential which modifies the wave function of the initial state particles and leads to a non-negligible correction of the tree-level cross section [46–49].

To leading order the effect of the QCD potential can be described by a Coulomb-like potential [50]

$$V(r) \approx \frac{\alpha_s}{2r}\left[C_Q - C_R - C_{R'}\right] \tag{B1}$$

where C_R and $C_{R'}$ denote the Casimir coefficients of the incoming particles while C_Q is the Casimir coefficient of the final state. For a general Coulomb-potential with $V(r) = \alpha/r$ the s-wave Sommerfeld correction factor S_0 is given by [46]

$$S_0 = -\frac{\pi\alpha/\beta}{1 - e^{\pi\alpha/\beta}}\,, \tag{B2}$$

where $\beta = v/2$ and the total annihilation cross section of particles moving in this potential is given by $\sigma_{Somm} = S_0 \cdot \sigma_{tree}$.[3] For final states which are exclusively in a singlet, i.e. $ZZ, W^+W^-, \gamma\gamma$, or an octet representation, i.e. $\gamma g, Zg$, the enhancement is given by Eq. (B2) with $\alpha = -4/3\alpha_s$ or $\alpha = 1/6\alpha_s$, respectively. The gg final state is slightly more complicated since it can be in a singlet or octet representation. After summing over the different contributions the total Sommerfeld correction factor for this case reads [46]

$$S_0 \to \frac{2}{7}S_0\Big|_{\alpha=-4/3\alpha_s} + \frac{5}{7}S_0\Big|_{\alpha=1/6\alpha_s}\,. \tag{B3}$$

Since this channel dominates the annihilation rates by orders of magnitude, we only take the correction for annihilation to gluons into account.

[3] In principle the Sommerfeld factors have to be determined separately for each partial wave. For the model considered here the total Sommerfeld effect can be approximated to good accuracy by applying the s-wave correction to the full cross section.

[1] G. Bertone, D. Hooper, and J. Silk, Phys. Rept., **405**, 279 (2005), arXiv:hep-ph/0404175 [hep-ph].
[2] G. Arcadi, M. Dutra, P. Ghosh, M. Lindner, Y. Mambrini, M. Pierre, S. Profumo, and F. S. Queiroz, (2017), arXiv:1703.07364 [hep-ph].
[3] K. Griest and D. Seckel, Phys. Rev., **D43**, 3191 (1991).
[4] D. J. H. Chung, G. R. Farrar, and E. W. Kolb, Phys. Rev., **D56**, 6096 (1997), arXiv:astro-ph/9703145 [astro-ph].
[5] J. Ellis, F. Luo, and K. A. Olive, JHEP, **09**, 127 (2015), arXiv:1503.07142 [hep-ph].
[6] M. Garny, A. Ibarra, M. Pato, and S. Vogl, JCAP, **1211**, 017 (2012), arXiv:1207.1431 [hep-ph].
[7] J. Edsjö and P. Gondolo, Phys. Rev., **D56**, 1879 (1997), arXiv:hep-ph/9704361.
[8] G. Belanger, F. Boudjema, A. Pukhov, and A. Semenov, Comput. Phys. Commun., **174**, 577 (2006), arXiv:hep-ph/0405253 [hep-ph].
[9] P. Gondolo, J. Edsjo, P. Ullio, L. Bergstrom, M. Schelke, and E. A. Baltz, JCAP, **0407**, 008 (2004), arXiv:astro-ph/0406204 [astro-ph].
[10] M. Backović, K. Kong, and M. McCaskey, Physics of the Dark Universe, **5-6**, 18 (2014), arXiv:1308.4955 [hep-ph].
[11] P. A. R. Ade *et al.* (Planck), Astron. Astrophys., **594**, A13 (2016), arXiv:1502.01589 [astro-ph.CO].
[12] L. J. Hall, K. Jedamzik, J. March-Russell, and S. M. West, JHEP, **03**, 080 (2010), arXiv:0911.1120 [hep-ph].
[13] G. R. Farrar and P. Fayet, Phys. Lett., **B76**, 575 (1978).
[14] S. Chatrchyan *et al.* (CMS), JHEP, **07**, 122 (2013), arXiv:1305.0491 [hep-ex].
[15] V. Khachatryan *et al.* (CMS), Tech. Rep. CMS-PAS-EXO-16-036 (2016).

[16] G. Aad *et al.* (ATLAS), JHEP, **01**, 068 (2015), arXiv:1411.6795 [hep-ex].
[17] M. Aaboud *et al.* (ATLAS), Phys. Rev., **D93**, 112015 (2016), arXiv:1604.04520 [hep-ex].
[18] V. Khachatryan *et al.* (CMS), Eur. Phys. J., **C75**, 325 (2015), arXiv:1502.02522 [hep-ex].
[19] J. Heisig, A. Lessa, and L. Quertenmont, JHEP, **12**, 087 (2015), arXiv:1509.00473 [hep-ph].
[20] J. Alwall, R. Frederix, S. Frixione, V. Hirschi, F. Maltoni, O. Mattelaer, H. S. Shao, T. Stelzer, P. Torrielli, and M. Zaro, JHEP, **07**, 079 (2014), arXiv:1405.0301 [hep-ph].
[21] T. Sjostrand, S. Mrenna, and P. Z. Skands, JHEP, **05**, 026 (2006), arXiv:hep-ph/0603175 [hep-ph].
[22] W. Beenakker, S. Brensing, M. Krämer, A. Kulesza, E. Laenen, and I. Niessen, JHEP, **08**, 098 (2010), arXiv:1006.4771 [hep-ph].
[23] A. C. Kraan, Eur. Phys. J., **C37**, 91 (2004), arXiv:hep-ex/0404001 [hep-ex].
[24] R. Mackeprang and A. Rizzi, Eur. Phys. J., **C50**, 353 (2007), arXiv:hep-ph/0612161 [hep-ph].
[25] Y. R. de Boer, A. B. Kaidalov, D. A. Milstead, and O. I. Piskounova, J. Phys., **G35**, 075009 (2008), arXiv:0710.3930 [hep-ph].
[26] R. Mackeprang and D. Milstead, Eur. Phys. J., **C66**, 493 (2010), arXiv:0908.1868 [hep-ph].
[27] G. Aad *et al.* (ATLAS), Phys. Rev., **D92**, 072004 (2015), arXiv:1504.05162 [hep-ex].
[28] G. Aad *et al.* (ATLAS), Phys. Rev., **D88**, 112006 (2013), arXiv:1310.3675 [hep-ex].
[29] V. Khachatryan *et al.* (CMS), JHEP, **01**, 096 (2015), arXiv:1411.6006 [hep-ex].
[30] R. Mahbubani, P. Schwaller, and J. Zurita, (2017), arXiv:1703.05327 [hep-ph].
[31] O. Buchmueller, A. De Roeck, M. McCullough, K. Hahn, K. Sung, P. Schwaller, and T.-T. Yu, (2017), arXiv:1704.06515 [hep-ph].
[32] A. M. Sirunyan *et al.* (CMS), (2017), arXiv:1704.07781 [hep-ex].
[33] V. Khachatryan *et al.* (CMS), Tech. Rep. CMS-PAS-SUS-16-036 (2017).
[34] A. M. Sirunyan *et al.* (CMS), (2016), arXiv:1612.03877 [hep-ex].
[35] M. Aaboud *et al.* (ATLAS), Eur. Phys. J., **C76**, 547 (2016), arXiv:1606.08772 [hep-ex].
[36] V. Khachatryan *et al.* (CMS), JHEP, **06**, 116 (2015), arXiv:1503.08037 [hep-ex].
[37] M. Aaboud *et al.* (ATLAS), Phys. Rev., **D94**, 032005 (2016), arXiv:1604.07773 [hep-ex].
[38] J. L. Feng, A. Rajaraman, and F. Takayama, Phys. Rev., **D68**, 063504 (2003), arXiv:hep-ph/0306024 [hep-ph].
[39] M. J. Baker *et al.*, JHEP, **12**, 120 (2015), arXiv:1510.03434 [hep-ph].
[40] A. Alloul, N. D. Christensen, C. Degrande, C. Duhr, and B. Fuks, Comput. Phys. Commun., **185**, 2250 (2014), arXiv:1310.1921 [hep-ph].
[41] A. Belyaev, N. D. Christensen, and A. Pukhov, Comput. Phys. Commun., **184**, 1729 (2013), arXiv:1207.6082 [hep-ph].
[42] S. Kim and M. Laine, JHEP, **07**, 143 (2016), arXiv:1602.08105 [hep-ph].
[43] S. Kim and M. Laine, JCAP, **1701**, 013 (2017), arXiv:1609.00474 [hep-ph].
[44] J. Hisano, S. Matsumoto, and M. M. Nojiri, Phys. Rev. Lett., **92**, 031303 (2004), arXiv:hep-ph/0307216 [hep-ph].
[45] J. Hisano, S. Matsumoto, M. M. Nojiri, and O. Saito, Phys. Rev., **D71**, 063528 (2005), arXiv:hep-ph/0412403 [hep-ph].
[46] A. De Simone, G. F. Giudice, and A. Strumia, JHEP, **06**, 081 (2014), arXiv:1402.6287 [hep-ph].
[47] A. Ibarra, A. Pierce, N. R. Shah, and S. Vogl, Phys. Rev., **D91**, 095018 (2015), arXiv:1501.03164 [hep-ph].
[48] A. Hryczuk, Phys. Lett., **B699**, 271 (2011), arXiv:1102.4295 [hep-ph].
[49] S. El Hedri, A. Kaminska, and M. de Vries, (2016), arXiv:1612.02825 [hep-ph].
[50] W. Fischler, Nucl. Phys., **B129**, 157 (1977).